Acta Mechanica 176, 45–60 (2005)
DOI 10.1007/s00707-004-0119-9

Acta Mechanica
Printed in Austria

Dynamic behavior of a crack in a functionally graded piezoelectric strip bonded to two dissimilar half piezoelectric material planes

J.-L. Sun, Z.-G. Zhou and **B. Wang,** Harbin, P.R. China

Received October 30, 2003; revised March 19, 2004
Published online: April 7, 2005

Summary. The dynamic behavior of a crack in a functionally graded piezoelectric material (FGPM) strip bonded to two half dissimilar piezoelectric material planes subjected to combined harmonic anti-plane shear wave and in-plane electrical loading was studied under the limited permeable and permeable electric boundary conditions. It was assumed that the elastic stiffness, piezoelectric constant and dielectric permittivity of the functionally graded piezoelectric layer vary continuously along the thickness of the strip. By using the Fourier transform, the problem can be solved with a set of dual integral equations in which the unknown variables are the jumps of the displacements and the electric potentials across the crack surfaces. In solving the dual integral equations, the jumps of the displacements and the electric potentials across the crack surfaces were expanded in a series of Jacobi polynomials. Numerical results illustrate the effects of the gradient parameter of FGPM, electric loading, wave number, thickness of FGPM strip and electric boundary conditions on the dynamic stress intensity factors (SIFs).

1 Introduction

Piezoelectric materials have been attractive materials for transducer and sensor applications due to the inherent electro-mechanical coupling behavior. However, most piezoelectric materials are brittle and many types of defects or cracks may be produced in piezoelectric materials during manufacturing processes. More and more piezoelectric devices are multi-layered, and they are susceptible to cracking due to uneven stress distributions or metal-to-ceramic bonds at which stress concentration occurs. Therefore,it is important to study the electro-elastic interaction and fracture behaviors of piezoelectric materials.

In recent years, researchers pay more attention to functionally graded materials (FGMs). FGMs are inhomogeneous materials which the material properties vary continuously in one or more directions. The concept of FGMs has been applied to piezoelectric materials to improve the reliability of piezoelectric materials and structures [1]–[3]. More recently, studies on fracture mechanic behavior of FGPMs have received some attention. Li and Weng [4] first considered the static anti-plane problem of a finite crack in an FGPM strip. They found that the singular stress and electric displacement at crack tips in an FGPM carry the same forms as those in a homogeneous piezoelectric material. It was also found that an increase in the gradient parameter of an FGPM could reduce the magnitude of the stress intensity factor. Wang [5] considered the anti-plane problem of an infinite FGPM. Ueda [6] solved the problem of a crack in an FGPM bonded to two elastic surface layers. Kwon [7] studied the electrical nonlinear behavior of an anti-plane shear crack in a functionally graded piezoelectric strip by using the strip saturation model within the framework of linear electro-elasticity. Chen et al. [8]–[9] solved the problem of transient response of a functionally graded piezoelectric medium for a through crack under the anti-plane or in-plane mechanical and electric impact. Some researchers [10]–[12] studied moving mode-III crack in FGPM. In Refs. [4]–[12], the unknown variables of dual integral equations were the dislocation density functions and the dual integral equations were solved by using the singular integral equation method. To our knowledge, no report was presented on dynamic behavior of a crack in an FGPM strip bonded to two dissimilar half piezoelectric material planes.

One important issue in studying fracture mechanics of piezoelectric materials is the electric boundary condition along the crack surfaces. There are two well-accepted electric boundary conditions: the permeable and impermeable boundary conditions. Some researchers [13]–[14] also suggested the boundary condition in the following form:

$$D_2^+ = D_2^-, D_2^+(u^+ - u^-) = \varepsilon_0(\phi^+ - \phi^-)$$

in which D_i, ϕ, ε_0 and $(u^+ - u^-)$ are the electric displacement component, the electric potential, the permittivity of air and the opening displacement component. This boundary condition will be reduced to the permeable boundary condition when $u^+ - u^- = 0$ and to the impermeable one when $\varepsilon_0 = 0$. Since no opening displacement $(u^+ - u^-)$ exists for the mode-III crack, this type of limited permeable electric boundary condition as mentioned above is not suitable for the mode-III crack problem in piezoelectric materials.

In this paper, in order to reveal the difference of these boundary conditions, the dynamic behavior of a mode-III crack in an FGPM strip bonded to two dissimilar half piezoelectric material planes was studied by use of the Schmidt method [15] under the limited permeable and permeable electric boundary conditions. By use of the Fourier transform, the problem could be solved with a set of dual integral equations in which the unknown variables are the jumps of the displacements and the electric potentials across the crack surfaces. In solving the dual integral equations, the jumps of the displacements and the electric potentials across the crack surfaces were expanded in a series of Jacobi polynomials. This process is quite different from those adopted in the Refs. [4]–[12] as mentioned above. Some numerical results are presented graphically to show the effects of the gradient parameter of the FGPM, wave number, electric loading, thickness of the FGPM strip and electric boundary conditions on the dynamic stress intensity factors.

2 Problem statement

Consider a crack of length $2a$ in an FGPM strip of width $h_1 + h_2$ bonded between two dissimilar half piezoelectric material planes. A Cartesian system (x, y, z) is positioned with its origin at the center of the crack. Note that the z-axis is oriented in the poling direction of the piezoelectric materials, and the xy-plane is the transversely isotropic plane, $x = 0$ is a plane of geometric symmetry, as shown in Fig. 1. The harmonic anti-plane mechanical and in-plane electrical waves are vertically incident. The mechanical and electrical fields corresponding to steady state incident waves can be expressed in terms of the frequency ω, such that $\tau_{yz}(x, y, t) = \tau_0 \exp(-i\omega t)$ and $D_y(x, y, t) = D_0 \exp(-i\omega t)$. For the sake of convenience, the time dependence of all field quantities assumed to be of the form $\exp(-i\omega t)$ will be suppressed and we only consider that τ_0 and D_0 are positive. Because of the assumed symmetry in geometry and loading, it is sufficient to consider the problem for $x > 0$, $-\infty < y < +\infty$ only.

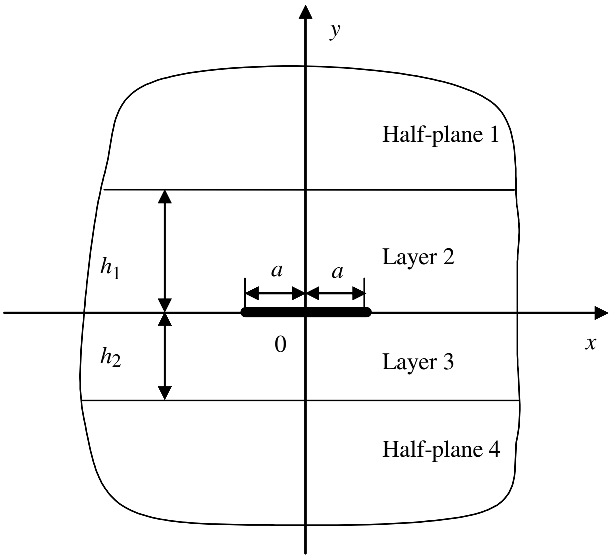

Fig. 1. Crack in functionally graded piezoelectric material

As shown in Fig. 1, we assume the material properties are described by [8]

$$\left(c_{44}^{(1)} \quad e_{15}^{(1)} \quad \varepsilon_{11}^{(1)} \quad \rho^{(1)}\right) = e^{\beta h_1}\left(c_{44}^{(0)} \quad e_{15}^{(0)} \quad \varepsilon_{11}^{(0)} \quad \rho^{(0)}\right), \quad y \geq h_1, \tag{1}$$

$$\left(c_{44}^{(k)} \quad e_{15}^{(k)} \quad \varepsilon_{11}^{(k)} \quad \rho^{(k)}\right) = e^{\beta y}\left(c_{44}^{(0)} \quad e_{15}^{(0)} \quad \varepsilon_{11}^{(0)} \quad \rho^{(0)}\right), \quad k = 2, 3, -h_2 \leq y \leq h_1, \tag{2}$$

$$\left(c_{44}^{(4)} \quad e_{15}^{(4)} \quad \varepsilon_{11}^{(4)} \quad \rho^{(4)}\right) = e^{-\beta h_2}\left(c_{44}^{(0)} \quad e_{15}^{(0)} \quad \varepsilon_{11}^{(0)} \quad \rho^{(0)}\right), \quad y \leq -h_2, \tag{3}$$

where $c_{44}^{(k)}$, $e_{15}^{(k)}$, $\varepsilon_{11}^{(k)}$ and $\rho^{(k)}$ are the shear modulus, the piezoelectric coefficient, the dielectric parameter and the mass density, while superscripts $k = 1, 2, 3, 4$ refer to the upper half plane 1, layer 2, layer 3 and lower half plane 4, respectively.

The constitutive equations of the anti-plane piezoelectric materials are

$$\tau_{jz}^{(k)} = \mu^{(k)} w_{,j}^{(k)} + e_{15}^{(k)} \psi_{,j}^{(k)}, \quad D_j^{(k)} = -\varepsilon_{11}^{(k)} \psi_{,j}^{(k)} \tag{4}$$

in which $\psi^{(k)} = \phi^{(k)} - \frac{e_{15}^{(k)}}{\varepsilon_{11}^{(k)}} w^{(k)}$, $\mu^{(k)} = c_{44}^{(k)} + \frac{e_{15}^{(k)2}}{\varepsilon_{11}^{(k)}}$ $(k = 1, 2, 3, 4, \ j = x, y)$, where $\psi^{(k)}$ is the Bleustein function [16], $\tau_{jz}^{(k)}$ and $D_j^{(k)}$ are the stress and electric displacement components, $w_{,j}^{(k)}$ is strain tensor, $\phi^{(k)}$ and $w^{(k)}$ are the electric potential and the mechanical displacement.

The dynamic anti-plane governing equations for homogeneous piezoelectric materials are given by

$$c_{44}^{(0)} \nabla^2 w^{(k)} + e_{15}^{(0)} \nabla^2 \phi^{(k)} = \rho^{(0)} \frac{\partial^2 w^{(k)}}{\partial t^2}, \tag{5}$$

$$e_{15}^{(0)} \nabla^2 w^{(k)} - \varepsilon_{11}^{(0)} \nabla^2 \phi^{(k)} = 0, \tag{6}$$

in which $\nabla^2 = \partial^2/x^2 + \partial^2/y^2$ is the two-dimensional Laplacian operator in the variables x and y. The dynamic anti-plane governing equations for functionally graded piezoelectric materials are given by

$$c_{44}^{(0)}\left(\nabla^2 + \beta\frac{\partial}{\partial y}\right) w^{(k)} + e_{15}^{(0)}\left(\nabla^2 + \beta\frac{\partial}{\partial y}\right)\phi^{(k)} = \rho^{(0)}\frac{\partial^2 w^{(k)}}{\partial t^2}, \tag{7}$$

$$e_{15}^{(0)}\left(\nabla^2+\beta\frac{\partial}{\partial y}\right)w^{(k)}-\varepsilon_{11}^{(0)}\left(\nabla^2+\beta\frac{\partial}{\partial y}\right)\phi^{(k)}=0. \tag{8}$$

The continuity boundary conditions can be stated as below

$$\begin{array}{ll}\tau_{yz}^{(1)}(x,h_1)=\tau_{yz}^{(2)}(x,h_1) & \phi^{(1)}(x,h_1)=\phi^{(2)}(x,h_1)\\ D_y^{(1)}(x,h_1)=D_y^{(2)}(x,h_1) & w^{(1)}(x,h_1)=w^{(2)}(x,h_1)\end{array},\qquad x>0 \tag{9}$$

$$\begin{array}{ll}\tau_{yz}^{(2)}(x,0)=\tau_{yz}^{(3)}(x,0) & \phi^{(2)}(x,0)=\phi^{(3)}(x,0)\\ D_y^{(2)}(x,0)=D_y^{(3)}(x,0) & w^{(2)}(x,0)=w^{(3)}(x,0)\end{array},\qquad x>a \tag{10}$$

$$\begin{array}{ll}\tau_{yz}^{(3)}(x,-h_2)=\tau_{yz}^{(4)}(x,-h_2) & \phi^{(3)}(x,-h_2)=\phi^{(4)}(x,-h_2)\\ D_y^{(3)}(x,-h_2)=D_y^{(4)}(x,-h_2) & w^{(3)}(x,-h_2)=w^{(4)}(x,-h_2)\end{array},\qquad x>0 \tag{11}$$

As discussed in [17], since the opening displacement is zero for the present anti-plane shear problem, the crack surfaces can be assumed to be in perfect contact. Accordingly, both the electric potential and normal electric displacement are assumed to be continuous across the crack surfaces. So the boundary conditions of the present problem are:

Case I:

$$\begin{array}{ll}\tau_{yz}^{(2)}(x,0)=\tau_{yz}^{(3)}(x,0)=-\tau_0 & D_y^{(2)}(x,0)=D_y^{(3)}(x,0)\\ \phi^{(2)}(x,0)=\phi^{(3)}(x,0) & \end{array},\qquad 0<x<a. \tag{12.1}$$

In order to reveal the difference between the limited permeable and permeable electric boundary conditions, the limited permeable electric boundary condition as given in the reference [10] is also considered in the present paper. It can be rewritten as follows:

Case II:

$$\tau_{yz}^{(2)}(x,0)=\tau_{yz}^{(3)}(x,0)=-\tau_0,\quad D_y^{(2)}(x,0)=D_y^{(3)}(x,0)=D_y^c-D_0\,,\quad 0<x<a, \tag{12.2}$$

where D_y^c and D_0 are the normal component of the electric displacement and electric loading on the crack faces.

From *case* II, it can be seen that the limited permeable electric boundary condition can be reduced to the impermeable electric boundary condition when $D_y^c=0$. However, it can not be reduced to the permeable electric boundary condition when $D_y^c=D_0$. It can be explained by the reason that, in this case, the electric potentials at crack surfaces are different.

By use of the Fourier cosine transforms, the solutions of the governing equations are as follows:

$$\begin{array}{l}w^{(1)}(x,y)=\frac{2}{\pi}\int_0^\infty A_1(s)e^{-\gamma y}\cos(sx)ds\\ \psi^{(1)}(x,y)=\frac{2}{\pi}\int_0^\infty C_1(s)e^{-sy}\cos(sx)ds\end{array},\quad y\geq h_1 \tag{13}$$

$$\begin{array}{l}w^{(k)}(x,y)=\frac{2}{\pi}\int_0^\infty [A_k(s)e^{m_1y}+B_k(s)e^{m_2y}]\cos(sx)ds\\ \psi^{(k)}(x,y)=\frac{2}{\pi}\int_0^\infty [C_k(s)e^{n_1y}+D_k(s)e^{n_2y}]\cos(sx)ds\end{array},\quad k=2,3,-h_2\leq y\leq h_1 \tag{14}$$

$$\begin{array}{l}w^{(4)}(x,y)=\frac{2}{\pi}\int_0^\infty B_4(s)e^{\gamma y}\cos(sx)ds\\ \psi^{(4)}(x,y)=\frac{2}{\pi}\int_0^\infty D_4(s)e^{sy}\cos(sx)ds\end{array},\quad y\leq -h_2 \tag{15}$$

where

$$m_1 = -\frac{\beta}{2} + \sqrt{\left(\frac{\beta}{2}\right)^2 + s^2 - \frac{\omega^2}{c^2}}, \quad m_2 = -\frac{\beta}{2} - \sqrt{\left(\frac{\beta}{2}\right)^2 + s^2 - \frac{\omega^2}{c^2}}, \quad n_1 = -\frac{\beta}{2} + \sqrt{\left(\frac{\beta}{2}\right)^2 + s^2},$$

$$n_2 = -\frac{\beta}{2} - \sqrt{\left(\frac{\beta}{2}\right)^2 + s^2}, \quad \gamma = \sqrt{s^2 - \frac{\omega^2}{c^2}}, c^2 = \mu^{(0)} \Big/ \rho^{(0)}, \quad \mu^{(0)} = c_{44}^{(0)} + e_{15}^{(0)2} \Big/ \varepsilon_{11}^{(0)}.$$

$A_k(s), C_k(s) (k = 1, 2, 3), B_k(s), D_k(s) (k = 2, 3, 4)$ are unknown functions to be determined from the boundary conditions.

Substituting those solutions into Eq. (4), one obtains the stress and electric displacement fields

$$\begin{aligned} \tau_{yz}^{(1)}(x,y) &= -\tfrac{2}{\pi} e^{\beta h_1} \int_0^\infty \left[\mu^{(0)} \gamma A_1(s) e^{-\gamma y} + e_{15}^{(0)} s C_1(s) e^{-sy} \right] \cos(sx) ds, \\ D_y^{(1)}(x,y) &= \tfrac{2}{\pi} e^{\beta h_1} \int_0^\infty \varepsilon_{11}^{(0)} s C_1(s) e^{-sy} \cos(sx) ds, \\ \phi^{(1)}(x,y) &= \tfrac{e_{15}^{(0)}}{\varepsilon_{11}^{(0)}} \tfrac{2}{\pi} \int_0^\infty A_1(s) e^{-\gamma y} \cos(sx) ds + \tfrac{2}{\pi} \int_0^\infty C_1(s) e^{-sy} \cos(sx) ds, \end{aligned} \tag{16}$$

$$\begin{aligned} \tau_{yz}^{(k)}(x,y) &= \tfrac{2}{\pi} e^{\beta y} \int_0^\infty \Big\{ \mu^{(0)} [m_1 A_k(s) e^{m_1 y} + m_2 B_k(s) e^{m_2 y}]. \\ &\qquad + e_{15}^{(0)} [n_1 C_k(s) e^{n_1 y} + n_2 D_k(s) e^{n_2 y}] \Big\} \cos(sx) ds, \\ D_y^{(k)}(x,y) &= -\tfrac{2}{\pi} e^{\beta y} \int_0^\infty \varepsilon_{11}^{(0)} [n_1 C_k(s) e^{n_1 y} + n_2 D_k(s) e^{n_2 y}] \cos(sx) ds, \\ \phi^{(k)}(x,y) &= \tfrac{e_{15}^{(0)}}{\varepsilon_{11}^{(0)}} \tfrac{2}{\pi} \int_0^\infty [A_k(s) e^{m_1 y} + B_k(s) e^{m_2 y}] \cos(sx) ds \\ &\qquad + \tfrac{2}{\pi} \int_0^\infty [C_k(s) e^{n_1 y} + D_k(s) e^{n_2 y}] \cos(sx) ds, \end{aligned} \tag{17}$$

$$\begin{aligned} \tau_{yz}^{(4)}(x,y) &= \tfrac{2}{\pi} e^{-\beta h_2} \int_0^\infty \left[\mu^{(0)} \gamma B_4(s) e^{\gamma y} + e_{15}^{(0)} s D_4(s) e^{sy} \right] \cos(sx) ds, \\ D_y^{(4)}(x,y) &= -\tfrac{2}{\pi} e^{-\beta h_2} \int_0^\infty \varepsilon_{11}^{(0)} s D_4(s) e^{sy} \cos(sx) ds, \\ \phi^{(4)}(x,y) &= \tfrac{e_{15}^{(0)}}{\varepsilon_{11}^{(0)}} \tfrac{2}{\pi} \int_0^\infty B_4(s) e^{\gamma y} \cos(sx) ds + \tfrac{2}{\pi} \int_0^\infty D_4(s) e^{sy} \cos(sx) ds. \end{aligned} \tag{18}$$

To solve the problem, the jumps of the displacements and the electric potentials across the crack surfaces are defined as follows:

$$f_w(x) = w^{(2)}(x,0) - w^{(3)}(x,0), \tag{19}$$

$$f_\phi(x) = \phi^{(2)}(x,0) - \phi^{(3)}(x,0). \tag{20}$$

Substituting Eqs. (14) and (17) into Eqs. (19)–(20), and applying Fourier cosine transforms with the boundary conditions, it can be obtained

Case I:

$$\overline{f_w}(s) = A_2(s) + B_2(s) - A_3(s) - B_3(s), \tag{21.1}$$

$$\overline{f_\phi}(s) = \frac{e_{15}^{(0)}}{\varepsilon_{11}^{(0)}} [A_2(s) + B_2(s) - A_3(s) - B_3(s)] + C_2(s) + D_2(s) - C_3(s) - D_3(s) = 0. \tag{21.2}$$

Case II:

$$\overline{f_w}(s) = A_2(s) + B_2(s) - A_3(s) - B_3(s), \tag{22.1}$$

$$\overline{f_\phi}(s) = \frac{e_{15}^{(0)}}{\varepsilon_{11}^{(0)}}[A_2(s) + B_2(s) - A_3(s) - B_3(s)] + C_2(s) + D_2(s) - C_3(s) - D_3(s). \tag{22.2}$$

By applying Fourier cosine transforms to Eqs. (13)–(18) with boundary conditions (9)–(12), it can be obtained

$$A_1(s)e^{-\gamma h_1} = A_2(s)e^{m_1 h_1} + B_2(s)e^{m_2 h_1}, \tag{23}$$

$$\frac{e_{15}^{(0)}}{\varepsilon_{11}^{(0)}}A_1(s)e^{-\gamma h_1} + C_1(s)e^{-sh_1} = \frac{e_{15}^{(0)}}{\varepsilon_{11}^{(0)}}\left[A_2(s)e^{m_1 h_1} + B_2(s)e^{m_2 h_1}\right] + C_2(s)e^{n_1 h_1} + D_2(s)e^{n_2 h_1} \tag{24}$$

$$\begin{aligned} &-\mu^{(0)}\gamma A_1(s)e^{-\gamma h_1} - e_{15}^{(0)} sC_1(s)e^{-sh_1} \\ &\quad = \mu^{(0)}\left[m_1 A_2(s)e^{m_1 h_1} + m_2 B_2(s)e^{m_2 h_1}\right] + e_{15}^{(0)}\left[n_1 C_2(s)e^{n_1 h_1} + n_2 D_2(s)e^{n_2 h_1}\right], \end{aligned} \tag{25}$$

$$sC_1(s)e^{-sh_1} = -\left[n_1 C_2(s)e^{n_1 h_1} + n_2 D_2(s)e^{n_2 h_1}\right], \tag{26}$$

$$\begin{aligned} &\mu^{(0)}[m_1 A_2(s) + m_2 B_2(s)] + e_{15}^{(0)}[n_1 C_2(s) + n_2 D_2(s)] \\ &\quad = \mu^{(0)}[m_1 A_3(s) + m_2 B_3(s)] + e_{15}^{(0)}[n_1 C_3(s) + n_2 D_3(s)], \end{aligned} \tag{27}$$

$$n_1 C_2(s) + n_2 D_2(s) = n_1 C_3(s) + n_2 D_3(s), \tag{28}$$

$$A_3(s)e^{-m_1 h_2} + B_3(s)e^{-m_2 h_2} = B_4(s)e^{-\gamma h_2}, \tag{29}$$

$$\frac{e_{15}^{(0)}}{\varepsilon_{11}^{(0)}}\left[A_3(s)e^{-m_1 h_2} + B_3(s)e^{-m_2 h_2}\right] + C_3(s)e^{-n_1 h_2} + D_3(s)e^{-n_2 h_2} = \frac{e_{15}^{(0)}}{\varepsilon_{11}^{(0)}}B_4(s)e^{-\gamma h_2} + D_4(s)e^{-sh_2}, \tag{30}$$

$$\begin{aligned} &\mu^{(0)}\left[m_1 A_3(s)e^{-m_1 h_2} + m_2 B_3(s)e^{-m_2 h_2}\right] + e_{15}^{(0)}\left[n_1 C_3(s)e^{-n_1 h_2} + n_2 D_3(s)e^{-n_2 h_2}\right] \\ &\quad = \mu^{(0)\gamma B_4(s)e^{-\gamma h_2} + e_{15}^{(0)} sD_4(s)e^{-sh_2}}, \end{aligned} \tag{31}$$

$$n_1 C_3(s)e^{-n_1 h_2} + n_2 D_3(s)e^{-n_2 h_2} = sD_4(s)e^{-sh_2}. \tag{32}$$

By solving the twelve equations (21) (*case I*) or (22) (*case II*) and (23)–(32) with twelve unknown functions $A_k(s)$, $C_k(s)$ (k =1,2,3), $B_k(s)$, $D_k(s)$ (k =2,3,4) and substituting the solutions into Eq. (17) and applying the boundary condition (12), it can be obtained

Case I:

$$\frac{2}{\pi}\int_0^\infty \overline{f_w}(s)\cos(sx)ds = 0, \quad x > a, \tag{33.1}$$

$$\frac{2}{\pi}\int_0^\infty s\Xi(s)\,\overline{f_w}(s)\cos(sx)ds = -\tau_0, \quad 0 < x < a. \tag{33.2}$$

Case II:

$$\frac{2}{\pi}\int_0^\infty \overline{f_w}(s)\cos(sx)ds = 0, \quad x > a, \tag{34.1}$$

$$\frac{2}{\pi}\int_0^\infty \overline{f_\phi}(s)\cos(sx)ds = 0, \quad x > a, \tag{34.2}$$

$$\frac{2}{\pi}\mu^{(0)}\int_0^\infty s\boldsymbol{\Omega}(s)\overline{f_w}(s)\cos(sx)ds = -\tau_0[1-\lambda_0(D_r-1)], \quad 0 < x < a, \tag{34.3}$$

$$\frac{2}{\pi}\int_0^\infty s\boldsymbol{\Psi}(s)\left[e_{15}^{(0)}\overline{f_w}(s) - \varepsilon_{11}^{(0)}\overline{f_\phi}(s)\right]\cos(sx)ds = \lambda_0\frac{\varepsilon_{11}^{(0)}}{e_{15}^{(0)}}\tau_0(D_r-1), \quad 0 < x < a, \tag{34.4}$$

where

$$D_r = D_y^c\Big/D_0,\ \lambda_0 = \frac{e_{15}^{(0)}D_0}{\varepsilon_{11}^{(0)}\tau_0} \quad \text{and} \quad \Xi(s) = -\frac{e_{15}^{(0)2}}{\varepsilon_{11}^{(0)}}\boldsymbol{\Psi}(s) + \mu^{(0)}\boldsymbol{\Omega}(s).$$

in which $\boldsymbol{\Psi}(s)$ and $\boldsymbol{\Omega}(s)$ are known functions and given in the Appendix.

3 Solution of the dual integral equations

The Schmidt method [18]–[20] is used to solve the dual integral equations (33) and (34). The jumps of the displacements and electric potentials are represented by the following series:

$$f_w(x) = \sum_{n=1}^{\infty} a_n\, P_{2n-2}^{\left(\frac{1}{2},\frac{1}{2}\right)}\left(\frac{x}{a}\right)\left(1-\frac{x^2}{a^2}\right)^{\frac{1}{2}}, \quad 0 < x \le a, \quad (\text{for } case\ I \text{ and } II) \tag{35.1}$$

$$f_\phi(x) = \sum_{n=1}^{\infty} b_n\, P_{2n-2}^{\left(\frac{1}{2},\frac{1}{2}\right)}\left(\frac{x}{a}\right)\left(1-\frac{x^2}{a^2}\right)^{\frac{1}{2}}, \quad 0 < x \le a, \quad (\text{for } case\ II,\ f_\phi(x) = 0 \text{ for } case\ I) \tag{35.2}$$

where a_n and b_n are unknown coefficients to be determined and $P_n^{(1/2,1/2)}(x)$ is a Jacobi polynomial [21]. The Fourier transform of Eq. (35) is [22]

$$\overline{f_w}(s) = \sum_{n=1}^{\infty} a_n G_n \frac{1}{s} J_{2n-1}(sa), \tag{36.1}$$

$$\overline{f_\phi}(s) = \sum_{n=1}^{\infty} b_n G_n \frac{1}{s} J_{2n-1}(sa), \tag{36.2}$$

where $G_n = 2\sqrt{\pi}(-1)^{n-1}\frac{\Gamma\left(2n-\frac{1}{2}\right)}{(2n-2)!}$. $\Gamma(x)$ and $J_n(x)$ are the Gamma and Bessel functions, respectively.

Substituting Eq. (36) into Eqs. (33) and (34), Eqs. (33.1) and (34.1,2) are automatically satisfied. The Eqs. (33.2) and (34.3, .4) reduce to the form after integration with respect to x for $[0, x]$

$$\sum_{n=1}^{\infty} a_n G_n \int_0^\infty \frac{1}{s}\Xi(s)J_{2n-1}(sa)\sin(sx)ds = -\frac{\pi\tau_0}{2}x, \qquad (\text{for } case\ I) \tag{37.1}$$

$$\sum_{n=1}^{\infty} a_n G_n \int_0^\infty \frac{1}{s}\boldsymbol{\Omega}(s)J_{2n-1}(sa)\sin(sx)ds = -\frac{\pi\tau_0}{2\mu^{(0)}}[1-\lambda_0(D_r-1)]x, \quad (\text{for } case\ II) \tag{37.2}$$

$$\sum_{n=1}^{\infty} c_n G_n \varepsilon_{11}^{(0)} \int_0^\infty \frac{1}{s}\boldsymbol{\Psi}(s)J_{2n-1}(sa)\sin(sx)ds = \frac{\pi\tau_0}{2}\lambda_0\frac{\varepsilon_{11}^{(0)}}{e_{15}^{(0)}}(D_r-1)x, \qquad (\text{for } case\ II) \tag{37.3}$$

where $c_n = \frac{e_{15}^{(0)}}{\varepsilon_{11}^{(0)}}a_n - b_n$.

From the relationship as in Gradshteyn and Ryzhik's work [21],

$$\int_0^\infty \frac{1}{s} J_n(s\xi)\sin(s\psi)ds = \begin{cases} \frac{\sin\left[n\sin^{-1}(\psi/\xi)\right]}{n}, & \xi > \psi \\ \frac{\xi^n \sin(n\pi/2)}{n\left[\psi+\sqrt{\psi^2-\xi^2}\right]^n}, & \psi > \xi \end{cases} \tag{38}$$

the semi-infinite integral in Eq. (37) can be modified as

$$\int_0^\infty \frac{1}{s}\Xi(s)J_{2n-1}(sa)\sin(sx)ds = \Xi_c \frac{1}{2n-1}\sin\left[(2n-1)\sin^{-1}\left(\frac{x}{a}\right)\right] + \int_0^\infty \frac{1}{s}[\Xi(s)-\Xi_c]J_{2n-1}(sa)\sin(sx)ds, \tag{39.1}$$

$$\int_0^\infty \frac{1}{s}\boldsymbol{\Omega}(s)J_{2n-1}(sa)\sin(sx)ds = \boldsymbol{\Omega}_c \frac{1}{2n-1}\sin\left[(2n-1)\sin^{-1}\left(\frac{x}{a}\right)\right] + \int_0^\infty \frac{1}{s}[\boldsymbol{\Omega}(s)-\boldsymbol{\Omega}_c]J_{2n-1}(sa)\sin(sx)ds, \tag{39.2}$$

$$\int_0^\infty \frac{1}{s}\boldsymbol{\Psi}(s)J_{2n-1}(sa)\sin(sx)ds = \boldsymbol{\Psi}_c \frac{1}{2n-1}\sin\left[(2n-1)\sin^{-1}\left(\frac{x}{a}\right)\right] + \int_0^\infty \frac{1}{s}[\boldsymbol{\Psi}(s)-\boldsymbol{\Psi}_c]J_{2n-1}(sa)\sin(sx)ds, \tag{39.3}$$

where $\Xi_c = \lim\limits_{s\to\infty}\Xi(s)$, $\boldsymbol{\Omega}_c = \lim\limits_{s\to\infty}\boldsymbol{\Omega}(s)$ and $\boldsymbol{\Psi}_c = \lim\limits_{s\to\infty}\boldsymbol{\Psi}(s)$ are given in the Appendix.

The integrands of the semi-infinite integral in Eq. (39) can be evaluated directly. Equation (37) can now be solved for the coefficients a_n and b_n by the Schmidt method. For brevity, Eq. (37.1) can be rewritten as (Eqs. (37.2,3) can be solved using similar method as following):

$$\sum_{n=1}^{\infty} a_n E_n(x) = U(x), \quad 0 < x < a, \tag{40}$$

where $E_n(x)$ and $U(x)$are known functions and the coefficients a_n are to be determined. A set of functions $P_n(x)$ which satisfy the orthogonality condition

$$\int_0^a P_m(x)P_n(x)dx = N_n\delta_{mn}, \quad N_n = \int_0^a P_n^2(x)dx \tag{41}$$

can be constructed from the function $E_n(x)$, such that

$$P_n(x) = \sum_{i=1}^{n} \frac{M_{in}}{M_{nn}} E_i(x), \tag{42}$$

where M_{ij} is the cofactor of the element d_{ij} of D_n, which is defined as

$$D_n = \begin{bmatrix} d_{11} & d_{12} & d_{13} & \dots & d_{1n} \\ d_{21} & d_{22} & d_{23} & \dots & d_{2n} \\ d_{31} & d_{32} & d_{33} & \dots & d_{3n} \\ \dots & \dots & \dots & \dots & \dots \\ d_{n1} & d_{n2} & d_{n3} & \dots & d_{nn} \end{bmatrix}, \quad d_{ij} = \int_0^a E_i(x)E_j(x)dx. \tag{43}$$

Using Eqs. (40)–(43), we obtain

$$a_n = \sum_{j=n}^{\infty} q_j \frac{M_{nj}}{M_{jj}} \quad \text{with} \quad q_j = \frac{1}{N_j}\int_0^a U(x)P_j(x)dx. \tag{44}$$

4 Field intensity factors

The coefficients a_n and b_n are known, so that the entire stress and the electric displacement fields can be obtained. $\tau_{yz}^{(k)}$ and $D_y^{(k)}$ along the crack line can be expressed, respectively, as
Case I:

$$\tau_{yz}^{(2)}(x,0) = \tau_{yz}^{(3)}(x,0) = \frac{2}{\pi}\sum_{n=1}^{\infty} a_n G_n \int_0^{\infty} \{\Xi_c + [\Xi(s) - \Xi_c]\} J_{2n-1}(sa)\cos(sx)ds, \tag{45.1}$$

$$D_y^{(2)}(x,0) = D_y^{(3)}(x,0) = \frac{2}{\pi}\sum_{n=1}^{\infty} a_n G_n \int_0^{\infty} e_{15}^{(0)} \{\Psi_c + [\Psi(s) - \Psi_c]\} J_{2n-1}(sa)\cos(sx)ds. \tag{45.2}$$

Case II:

$$\tau_{yz}^{(2)}(x,0) = \tau_{yz}^{(3)}(x,0) = \frac{2}{\pi}\sum_{n=1}^{\infty} a_n G_n \int_0^{\infty} \{\Xi_c + \Xi(s) - \Xi_c\} J_{2n-1}(sa)\cos(sx)ds$$
$$+ \frac{2}{\pi}\sum_{n=1}^{\infty} b_n G_n \int_0^{\infty} e_{15}^{(0)} \{\Psi_c + [\Psi(s) - \Psi_c]\} J_{2n-1}(sa)\cos(sx)ds, \tag{46.1}$$

$$D_y^{(2)}(x,0) = D_y^{(3)}(x,0) = \frac{2}{\pi}\sum_{n=1}^{\infty} a_n G_n \int_0^{\infty} e_{15}^{(0)} \{\Psi_c + [\Psi(s) - \Psi_c]\} J_{2n-1}(sa)\cos(sx)ds$$
$$- \frac{2}{\pi}\sum_{n=1}^{\infty} b_n G_n \int_0^{\infty} \varepsilon_{11}^{(0)} \{\Psi_c + [\Psi(s) - \Psi_c]\} J_{2n-1}(sa)\cos(sx)ds. \tag{46.2}$$

From the relationship [21],

$$\int_0^{\infty} J_n(s\xi)\cos(s\psi)ds = \begin{cases} \frac{\cos\left[n\sin^{-1}(\psi/\xi)\right]}{\sqrt{\xi^2-\psi^2},}, & \xi > \psi \\ -\frac{\xi^n \sin(n\pi/2)}{\sqrt{\psi^2-\xi^2}\left[\psi+\sqrt{\psi^2-\xi^2}\right]^n}, & \psi > \xi \end{cases} \tag{47}$$

the singular part of the stress field and the singular part of the electric displacement field can be expressed as follows:
Case I:

$$\tau_{yz}^{(2)} = -\frac{2\Xi_c}{\pi}\sum_{n=1}^{\infty} a_n G_n H_n(x), \qquad \text{for } x > a, \tag{48.1}$$

$$D_y^{(2)} = -e_{15}^{(0)}\frac{2\Psi_c}{\pi}\sum_{n=1}^{\infty} a_n G_n H_n(x), \quad \text{for } x > a. \tag{48.2}$$

Case II:

$$\tau_{yz}^{(2)} = -\frac{2}{\pi}\Xi_c \sum_{n=1}^{\infty} a_n G_n H_n(x) - \frac{2}{\pi}\boldsymbol{\Psi}_c e_{15}^{(0)} \sum_{n=1}^{\infty} b_n G_n H_n(x)$$
$$= -\frac{2}{\pi}\sum_{n=1}^{\infty}\left\{a_n \Xi_c + b_n e_{15}^{(0)} \boldsymbol{\Psi}_c\right\} G_n H_n(x), \qquad \text{for } x > a, \tag{49.1}$$

$$D_y^{(2)} = -\frac{2}{\pi} e_{15}^{(0)} \boldsymbol{\Psi}_c \sum_{n=1}^{\infty} a_n G_n H_n(x) + \frac{2}{\pi}\varepsilon_{11}^{(0)} \boldsymbol{\Omega}_c \sum_{n=1}^{\infty} b_n G_n H_n(x)$$
$$= -\frac{2}{\pi}\sum_{n=1}^{\infty}\left[e_{15}^{(0)} \Xi_c a_n - \varepsilon_{11}^{(0)} \Xi_c b_n\right] G_n H_n(x), \quad \text{for } x > a, \tag{49.2}$$

where $H_n(x) = \frac{(-1)^{n-1} a^{2n-1}}{\sqrt{x^2-a^2}\left[x+\sqrt{x^2-a^2}\right]^{2n-1}}$.

We obtain the stress intensity factors as
Case I:

$$K_{III} = \lim_{x\to a^+} \sqrt{2\pi(x-a)}\,\tau_{yz}^{(2)} = -\frac{4\Xi_c}{\sqrt{a}}\sum_{n=1}^{\infty} a_n \frac{\Gamma\left(2n-\frac{1}{2}\right)}{(2n-2)!} = \frac{2}{\sqrt{a}}\sum_{n=1}^{\infty} a_n c_{44}^{(0)} \frac{\Gamma\left(2n-\frac{1}{2}\right)}{(2n-2)!}. \tag{50}$$

Case II:

$$K_{III} = \lim_{x\to a^+} \sqrt{2\pi(x-a)}\,\tau_{yz}^{(2)} = -\frac{4}{\sqrt{a}}\sum_{n=1}^{\infty}\left\{a_n \Xi_c + e_{15}^{(0)} \boldsymbol{\Psi}_c b_n\right\} \frac{\Gamma\left(2n-\frac{1}{2}\right)}{(2n-2)!}.$$
$$= \frac{2}{\sqrt{a}}\sum_{n=1}^{\infty}\left\{c_{44}^{(0)} a_n + e_{15}^{(0)} b_n\right\} \frac{\Gamma\left(2n-\frac{1}{2}\right)}{(2n-2)!}. \tag{51}$$

We obtain the electric displacement intensity factors as
Case I:

$$D_{III} = \lim_{x\to a^+} \sqrt{2\pi(x-a)}\,D_y^{(2)} = \frac{2}{\sqrt{a}}\sum_{n=1}^{\infty} e_{15}^{(0)} a_n \frac{\Gamma\left(2n-\frac{1}{2}\right)}{(2n-2)!} = \frac{e_{15}^{(0)}}{c_{44}^{(0)}} K_{III}. \tag{52}$$

Case II:

$$D_{III} = \lim_{x\to a^+} \sqrt{2\pi(x-a)}\,D_y^{(2)} = \frac{2}{\sqrt{a}}\sum_{n=1}^{\infty}\left[e_{15}^{(0)} a_n - \varepsilon_{11}^{(0)} b_n\right] \frac{\Gamma\left(2n-\frac{1}{2}\right)}{(2n-2)!}. \tag{53}$$

5 Numerical calculations and discussion

From the works [23]–[25] it can be seen that the Schmidt method is performed satisfactorily if the first ten terms of the infinite series in Eq. (40) are obtained. To examine the effect of electro-elastic coupling properties on the dynamic stress intensity factors, the solutions of the field equations have been computed numerically. The material along the plane $y = 0$ is assumed to be commercially available piezoelectric ceramic PZT-4. The material constants are $c_{44}^{(0)} = 2.56 \times 10^{10}\,\mathrm{N/m^2}, e_{15}^{(0)} = 12.7\,\mathrm{C/m^2}, \varepsilon_{11}^{(0)} = 64.6 \times 10^{-10}\,\mathrm{C/Vm}$.

From the results in Figs. 2–8, the following observations are very significant:

(i) From Eqs. (50)–(53), it can be given that the stress and electric displacement fields near the crack tips in FGPMs still possess the square root singularity as discussed in [4].

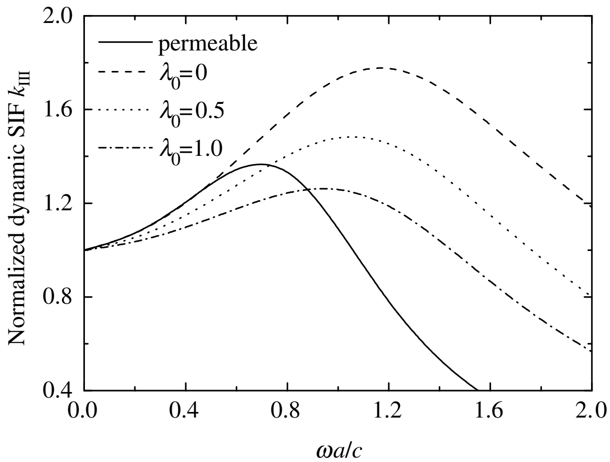

Fig. 2. The normalized dynamic SIFs versus $\omega a/c$ for $h_1/a = h_2/a = 0.5$ and $\beta a = 0$ (permeable and impermeable)

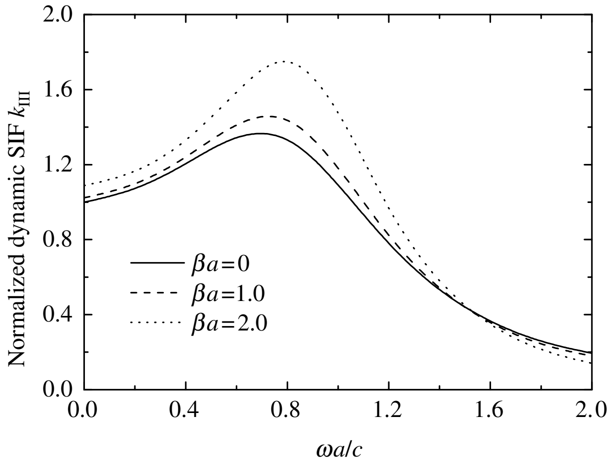

Fig. 3. The normalized dynamic SIFs versus $\omega a/c$ for $h_1/a = h_2/a = 0.5$ (*case I*)

(ii) Figure 2 displays the normalized dynamic SIFs $k_{III} = K_{III}/(\tau_0\sqrt{\pi a})$versus the wave number $\omega a/c$ for homogeneous piezoelectric material ($\beta a = 0$) under permeable and impermeable ($D_r = 0$) electric boundary conditions. From this figure, it can be seen that the numerical results of normalized dynamic SIFs are the same as the results investigated by Wang and Meguid [26] using the integral equation method.

(iii) Figures 3 and 4 show the effect of the wave number $\omega a/c$ under different βa and D_r on the normalized dynamic SIFs for *case I* and *II*. It can be seen that the normalized dynamic SIFs increase with the increase of the wavenumber $\omega a/c$ until they reach a peak value, and then decrease with the increase of $\omega a/c$. The present results show a similar trend to those for inhomogeneous materials without piezoelectric effect.

(iv) Figure 4 shows the effect of the electric boundary condition D_r on the normalized dynamic SIFs for $h_1/a = h_2/a = 0.5, \lambda_0 = 1.0$ and $\beta a = 1.0$ for *case I* and *II*. From this figure, it can be seen that the normalized dynamic SIFs increase with increasing D_r. However, the results of the normalized dynamic SIFs under permeable electric boundary condition are different from ones under limited permeable electric boundary condition when $D_r = 1.0$. The reason is that the electric potential is not continuous across the crack surfaces under limited permeable electric boundary condition.

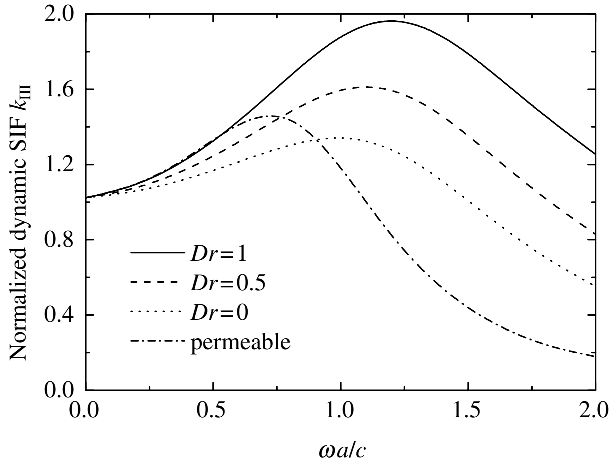

Fig. 4. The normalized dynamic SIFs versus $\omega a/c$ for $h_1/a = h_2/a = 0.5$, $\lambda_0 = 1.0$ and $\beta a = 1.0$ (*case I* and *II*)

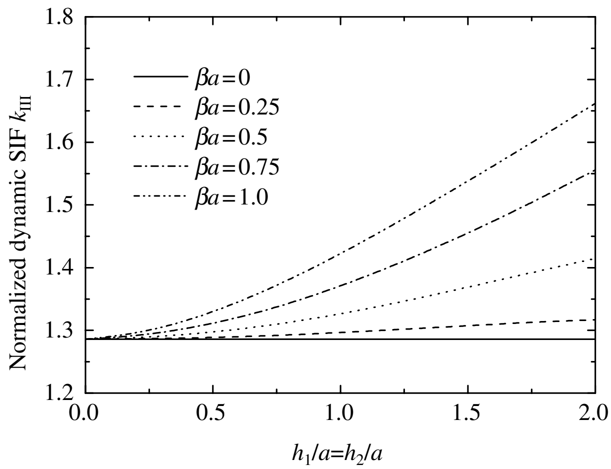

Fig. 5. The normalized dynamic SIFs versus $h_1/a = h_2/a$ for $\omega a/c = 0.5$ (*case I*)

(iv) Figures 5 and 6 illustrate the variations of the normalized dynamic SIFs with the thickness of the FGPM layer $(h_1 + h_2)/a$ under different βa. It is observed that the normalized dynamic SIFs increase with the increasing of $h_1/a = h_2/a$ under different $\beta a \neq 0$. When $\beta a = 0$, the normalized dynamic SIFs keep steady values. It can be explained by the reason that, in this case, the crack lies in a homogeneous piezoelectric infinite plane and the effects of $h_1/a = h_2/a$ on the normalized dynamic SIFs vanish.

(vi) Figures 7 and 8 show the effect of the thickness of the FGPM layer h_1/a and h_2/a on the normalized dynamic SIFs under different βa. Figure 7 displays the normalized dynamic SIFs versus h_1/a for $\omega a/c = 0.5, D_r = 0.5, h_2/a = 1.0$ and $\lambda_0 = 2.0$. The normalized dynamic SIFs decrease with the increase of h_1/a, then they tend to keep steady value as shown in Fig. 7. It can be explained by the reasons that, as h_1/a is increasing, the material of upper half plane becomes "harder" while the material of the lower half plane does not change. Figure 8 shows the normalized dynamic SIFs versus h_2/a for $\omega a/c = 0.5, D_r = 0.5, h_1/a = 1.0$ and $\lambda_0 = 2.0$. From this figure, it can be seen that the normalized dynamic SIFs increase with the increase of $h_2/a = 1.0$, and then tend to keep steady. The reason of those results shown in Fig. 8 is that, as h_2/a is increasing, the

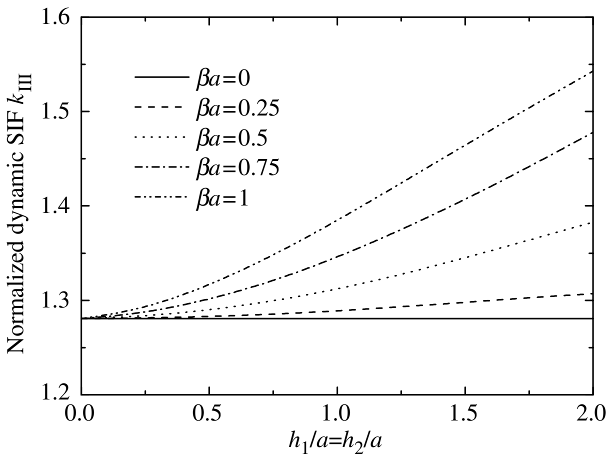

Fig. 6. The normalized dynamic SIFs versus $h_1/a = h_2/a$ for $\omega a/c = 0.5$, $D_r = 0.5$ and $\lambda_0 = 2.0$ (*case II*)

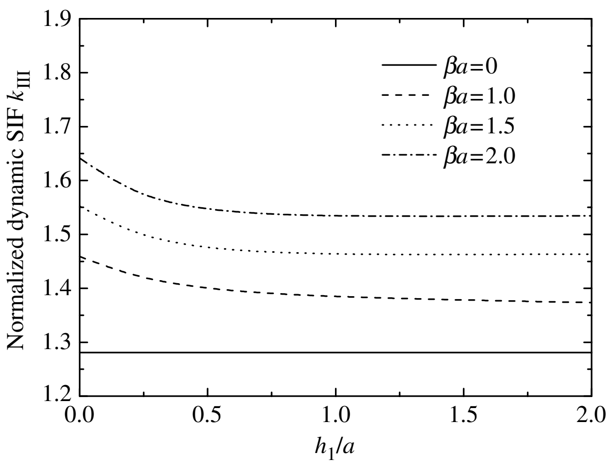

Fig. 7. The normalized dynamic SIFs versus h_1/a for $\omega a/c = 0.5$, $D_r = 0.5$, $h_2/a = 1.0$ and $\lambda_0 = 2.0$ (*case II*)

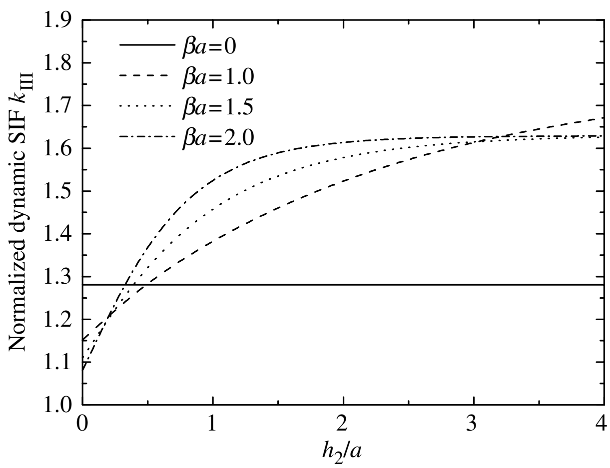

Fig. 8. The normalized dynamic SIFs versus h_2/a for $\omega a/c = 0.5$, $D_r = 0.5$, $h_1/a = 1.0$ and $\lambda_0 = 2.0$ (*case II*)

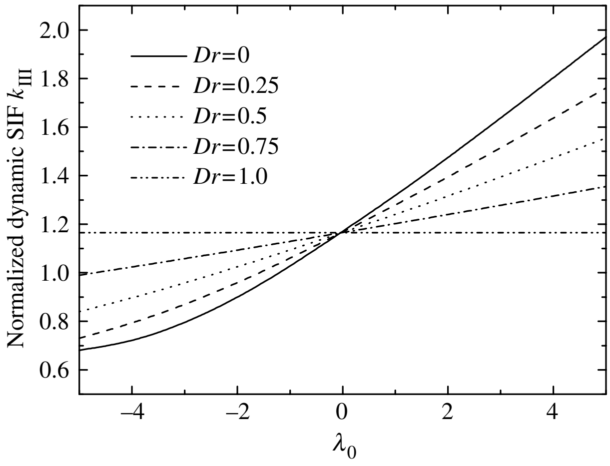

Fig. 9. The normalized dynamic SIFs versus λ_0 for $\omega a/c = 0.5$, $h_1/a = h_2/a = 0.5$ and $\beta a = 1.0$ (*case II*)

material of lower half plane becomes "softer" while the material of the upper half plane does not change.

(vii) Figure 9 shows the effect of electric loading λ_0 under different D_r on normalized dynamic SIFs. It can be seen that the effect of external electric loading upon the normalized dynamic SIFs becomes smaller as D_r is increasing. Especially, when $D_r = 1.0$, the electric loading has no effect on normalized dynamic SIFs. The explanation for this phenomenon is that, in this case, the external electric displacement loading is continuous across the crack surfaces.

(viii) Figures 3 and 5–8 also show the effect of the gradient parameter of the FGPM βa on normalized dynamic SIFs. It can be obtained that the normalized dynamic SIFs increase with increasing βa. This means that by decreasing the gradient parameter of FGPMs, the dynamic stress intensity factors can be reduced.

(ix) Based on the numerical calculation outlined above, it can be concluded that the normalized dynamic SIFs depend on the gradient parameter of the FGPM, thickness of the FGPM layers, electric boundary condition, wave number and electric loading.

Appendix

$$\Psi(s) = \frac{\alpha(s)}{\beta(s)}, \quad \Omega(s) = \frac{\chi(s)}{\delta(s)},$$

$$\alpha(s) = [\alpha_1(s) + \alpha_2(s)][\alpha_3(s) + \alpha_4(s)], \quad \alpha_1(s) = e^{h_2(n_2-n_1)}N_2(N_1 - 1), \quad \alpha_2(s) = -N_1(N_2 - 1),$$

$$\alpha_3(s) = N_2(N_1 + 1), \quad \alpha_4(s) = -e^{h_2(n_2-n_1)}N_1(N_2 + 1), \quad \beta(s) = (N_1 - N_2)[\beta_1(s) + \beta_2(s)],$$

$$\beta_1(s) = (N_2 - 1)(N_1 + 1), \quad \beta_2(s) = -e^{(h_1+h_2)(n_2-n_1)}(N_1 - 1)(N_2 + 1),$$

$$\chi(s) = [\chi_1(s) + \chi_2(s)][\chi_3(s) + \chi_4(s)], \quad \chi_1(s) = -e^{h_2(m_2-m_1)}M_2(M_1 - \Lambda), \quad \chi_2(s) = M_1(M_2 - \Lambda),$$

$$\chi_3(s) = M_2(M_1 + \Lambda), \quad \chi_4(s) = -e^{h_1(m_2-m_1)}M_1(M_2 + \Lambda), \quad \delta(s) = (M_1 - M_2)[\delta_1(s) + \delta_2(s)],$$

$$\delta_1(s) = (M_2 - \Lambda)(M_1 + \Lambda), \quad \delta_2(s) = -e^{(h_1+h_2)(m_2-m_1)}(M_1 - \Lambda)(M_2 + \Lambda)$$

$$\Psi_c = \lim_{s\to\infty} \Psi(s) = \frac{\alpha_c}{\beta_c} = -\frac{1}{2}, \ \ \Omega_c = \lim_{s\to\infty} \Omega(s) = \frac{\chi_c}{\delta_c} = -\frac{1}{2}, \ \ \Xi_c = -\frac{e_{15}^{(0)2}}{\varepsilon_{11}^{(0)}}\Psi_c + \mu^{(0)}\Omega_c = -\frac{1}{2}c_{44}^{(0)},$$

where

$$M_1 = -\frac{\beta}{2s} + \sqrt{\left(\frac{\beta}{2}\right)^2 \frac{1}{s^2} + 1 - \frac{\omega^2}{c^2 s^2}}, \quad M_2 = -\frac{\beta}{2s} - \sqrt{\left(\frac{\beta}{2}\right)^2 \frac{1}{s^2} + 1 - \frac{\omega^2}{c^2 s^2}}\,,$$

$$N_1 = -\frac{\beta}{2s} + \sqrt{\left(\frac{\beta}{2}\right)^2 \frac{1}{s^2} + 1}, \quad N_2 = -\frac{\beta}{2s} - \sqrt{\left(\frac{\beta}{2}\right)^2 \frac{1}{s^2} + 1}, \quad \Lambda = \sqrt{1 - \frac{\omega^2}{c^2 s^2}}\,.$$

Acknowledgements

The authors wish to thank the National Natural Science Foundation of China (10172030; 50322030), the Natural Science Foundation with Excellent Yound Investigators of Hei Long Jiang Procince (JC04-08) and the National Natural Science Foundation of Hei Long Jiang province (A0301).

Reference

[1] Zhu, X. H., Meng, Z. Y.: Operational principle, fabrication and displacement characteristics of a functionally gradient piezoelectric ceramic actuator. Sensor. Actuat. A. **48,** 169–173 (1996).
[2] Zhu, X., Zhu, J., Zhou, S., Li, Q., Liu, Z.: Microstructures of the monomorph piezoelectric ceramic actuators with functionally gradient. Sensor. Actuat. A. **74,** 198–202 (1999).
[3] Takagi, K., Li, J. F., Yokoyama, S., Watanabe, R., Almajid, A., Taya, M.: Design and fabrication of functionally graded PZT/Pt piezoelectric bimorph actuator. Sci. Technol. Adv. Mater. **3,** 217–224 (2002).
[4] Li, C., Weng, G. J.: Antiplane crack problem in functionally graded piezoelectric materials. ASME J. Appl. Mech. **69,** 481–488 (2002).
[5] Wang, B. L.: A mode-III crack in functionally graded piezoelectric materials. Mech. Res. Commun. **30,** 151–159 (2003).
[6] Ueda, S.: Crack in functionally graded piezoelectric strip bonded to elastic surface layers under electromechanical loading. Theor. Appl. Fract. Mech. **40** 225–236 (2003).
[7] Kwon, S. M.: Electrical nonlinear anti-plane shear crack in a functionally graded piezoelectric strip. Int. J. Solids Struct. **40,** 5649–5667 (2003).
[8] Chen, J., Liu, Z., Zou, Z.: Dynamic response of a crack in a functionally graded interface of two dissimilar piezoelectric half-planes. Arch. Appl. Mech. **72,** 686–696 (2003).
[9] Chen, J., Liu, Z. X., Zou, Z. Z.: Electromechanical impact of a crack in a functionally graded piezoelectric medium. Theor. Appl. Fract. Mech. **39,** 47–60 (2003).
[10] Kwon, S. M., Lee, K. Y.: An anti-plane propagating crack in a functionally graded piezoelectric strip bonded to a homogeneous piezoelectric strip. Arch. Appl. Mech. **73,** 348–366 (2003).
[11] Jin, B., Zhong, Z.: A moving mode-III crack in functionally graded piezoelectric material: permeable problem. Mech. Res. Commun. **29,** 217–224 (2002).
[12] Li, C., Weng, G. J.: Yoffe-type moving crack in a functionally graded piezoelectric material. Proc. Royal Soc. London A **458,** 381–399 (2002).
[13] Hao, T. -H., Shen, Z. -Y.: A new electric boundary condition of electric fracture mechanics and its applications. Eng. Fract. Mech. **47,** 793–802 (1994).
[14] Dascalu, C., Homentcovschi, D.: An intermediate crack model for flaws in piezoelectric solids. Acta Mech. **154,** 85–100 (2002).
[15] Morse, P. M., Feshbach, H.: Methods of theoretical physics. New York: McGraw-Hill 1958.

[16] Bleustein, J. L.: A new surface wave in piezoelectric materials. Appl. Phys. Lett. **13,** 412–413 (1968).
[17] Soh, A. K., Fang, D. N., Lee, K. L.: Analysis of a bi-piezoelectric ceramic layer with an interfacial crack subjected to anti-plane shear and in-plane electric loading. Eur. J. Mech. A/Solid **19,** 961–977 (2000).
[18] Zhou, Z. G., Wang, B.: The behavior of two parallel symmetry permeable interface cracks in a piezoelectric layer bonded to two half piezoelectric materials planes. Int. J. Solids Struct. **39,** 4485–4500 (2002).
[19] Itou, S.: Transient dynamic stress intensity factors around a crack in a nonhomogeneous interfacial layer between two dissimilar elastic half-planes. Int. J. Solids Struct. **38,** 3631–3645 (2001).
[20] Itou, S., Haliding, H.: Dynamic stress intensity factors around two parallel cracks in an infinite-orthotropic plane subjected to incident harmonic stress waves. Int. J. Solids Struct. **34,** 1145–1165 (1997).
[21] Gradshteyn, I. S., Ryzhik, I. M.: Table of integral, series and products. New York: Academic Press 1980.
[22] Erdelyi, A.: Tables of integral transforms. New York: McGraw-Hill 1954.
[23] Itou, S., Shima, Y.: Stress intensity factors around a cylindrical crack in an interfacial zone in composite materials. Int. J. Solids Struct. **36,** 697–709 (1999).
[24] Zhou, Z. -G., Han, J. -C., Du, S. -Y.: Investigation of a crack subjected to anti-plane shear by using the non-local theory. Int. J. Solids Struct. **36,** 3891–3901 (1999).
[25] Zhou, Z. -G., Bai, Y. -Y., Zhang, X. -W.: Two collinear Griffith cracks subjected to uniform tension in infinitely strip. Int. J. Solids Struct. **36,** 5597–5609 (1999).
[26] Wang, X. D., Meguid, S. A.: Modelling and analysis of the dynamic behavior of piezoelectric materials containing interacting cracks. Mech. Mater. **32,** 723–737 (2000).

Authors' address: J.-L. Sun, Z.-G. Zhou and B. Wang, Center for Composite Materials and Electro-Optics Technology Center, P.O. Box 1247, Harbin Institute of Technology, Harbin, 150001, P. R. China (E-mail: jlsun@hit.edu.cn)